INTERFACE

royalsocietypublishing.org/journal/rsif

Research

Cite this article: Johnston ST, Faria M, Crampin EJ. 2020 Isolating the sources of heterogeneity in nano-engineered particle–cell interactions. *J. R. Soc. Interface* **17**: 20200221. http://dx.doi.org/10.1098/rsif.2020.0221

Received: 1 April 2020
Accepted: 20 April 2020

Subject Category:
Life Sciences–Mathematics interface

Subject Areas:
nanotechnology, biomathematics

Keywords:
cell heterogeneity, nano-engineered particles, mathematical modelling, particle–cell interactions, cell cycle

Author for correspondence:
Stuart T. Johnston
e-mail: stuart.johnston@unimelb.edu.au

Electronic supplementary material is available online at https://doi.org/10.6084/m9.figshare.c.4966271.

THE ROYAL SOCIETY PUBLISHING

Isolating the sources of heterogeneity in nano-engineered particle–cell interactions

Stuart T. Johnston[1,2], Matthew Faria[1,2] and Edmund J. Crampin[1,2,3]

[1]Systems Biology Laboratory, School of Mathematics and Statistics, and Department of Biomedical Engineering, [2]ARC Centre of Excellence in Convergent Bio-Nano Science and Technology, Melbourne School of Engineering, and [3]School of Medicine, Faculty of Medicine Dentistry and Health Sciences, University of Melbourne, Parkville, Victoria 3010, Australia

STJ, 0000-0003-4532-5573

Nano-engineered particles have the potential to enhance therapeutic success and reduce toxicity-based treatment side effects via the targeted delivery of drugs to cells. This delivery relies on complex interactions between numerous biological, chemical and physical processes. The intertwined nature of these processes has thus far hindered attempts to understand their individual impact. Variation in experimental data, such as the number of particles inside each cell, further inhibits understanding. Here, we present a mathematical framework that is capable of examining the impact of individual processes during particle delivery. We demonstrate that variation in experimental particle uptake data can be explained by three factors: random particle motion; variation in particle–cell interactions; and variation in the maximum particle uptake per cell. Without all three factors, the experimental data cannot be explained. This work provides insight into biological mechanisms that cause heterogeneous responses to treatment, and enables precise identification of treatment-resistant cell subpopulations.

1. Introduction

Elucidating how individual biological and physical processes dictate the successful cellular uptake of nano-engineered particles is crucial for future developments in areas such as nanomedicine and nanotoxicology [1,2]. Untangling the role of a particular process requires a detailed understanding of the complex marriage of transport phenomena, physico-chemical particle characteristics and biological behaviour that govern particle–cell interactions [1–4]. It is well established that the physico-chemical properties of a nano-engineered particle, such as size, shape and surface charge, impact particle uptake [1,2,4,5]. Note that we use the terminology of nano-engineered particles to follow the Food and Drug Administration definition of nanotechnology: 'products that contain or are manufactured using materials in the nanoscale range [6].' This is in contrast to referring to the particles as nanoparticles, as this may imply than the particles are less than 100 nm in diameter. The exact influence of the physico-chemical properties of particles on uptake is unclear, as the impact is obscured by both the influence of transport phenomena, such as sedimentation, diffusion and aggregation, and cell-type specific interactions between cells and particles [4,7–9]. The inherent variation in cell characteristics within a population further obscures the roles of individual processes, and results in heterogeneous experimental data [10–14].

Heterogeneity in experimental data may imply that commonly reported population-averaged measures do not accurately reflect the underlying biology [15–17]. For example, consider a particle–cell association assay, where the average number of particles associated with a cell is measured after exposure to a particular concentration of particles [8]. This measure, referred to as particle dose, can be used as a proxy for the effectiveness of a putative treatment [18]. Effective treatment of disease via drug-loaded particles may require universal cellular uptake within a population [13], such that all cells interact with the drug. Reporting only the average number of associated particles does not distinguish between the influence of stochastic processes, where all cells are identical but associate

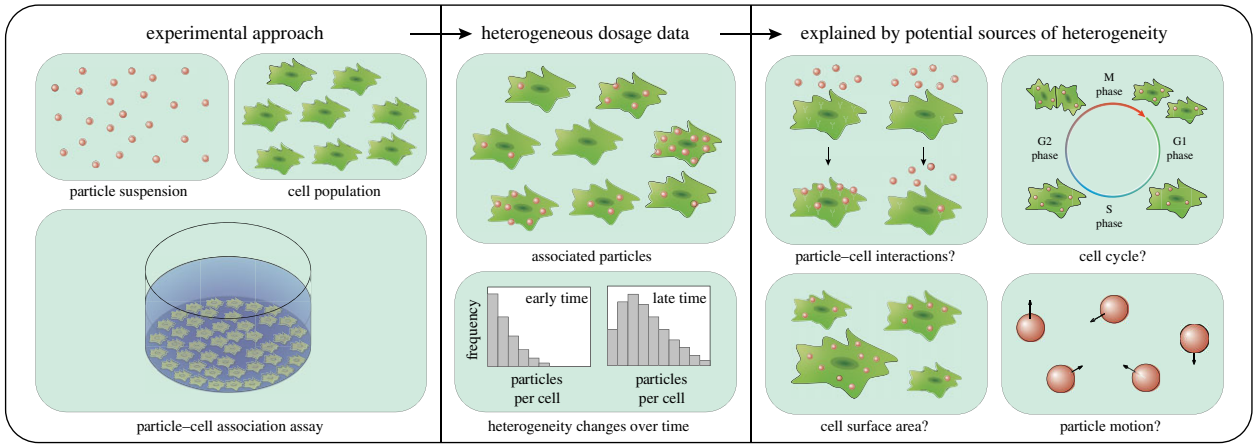

Figure 1. Schematic highlighting the experimental approach that gives rise to a heterogeneous dosage distribution with potential sources of heterogeneity. Particle-cell association assays result in heterogeneous dosage distributions, which may be explained by heterogeneity in (i) particle–cell interactions; (ii) the cell cycle; (iii) cell surface area; or (iv) stochastic particle motion.

with particles at random, and the presence of distinct subpopulations of cells that interact differently with particles due to fundamental differences in biology (figure 1). Certain cell subpopulations may not associate with particles, or associate with particles at an inhibited rate [13]. Even if such cell subpopulations are rare, they can nevertheless have a substantial impact on disease progression [15,19,20]. Identifying whether a cell population does, in fact, contain heterogeneity in relevant cell characteristics or whether variation in experimental data is merely a by-product of the stochastic nature of particle transport is therefore critical for therapeutic success [10–14]. Furthermore, understanding how heterogeneity in cell characteristics, such as receptor numbers or vesicle formation rates, manifests itself in commonly measured experimental data is crucial for isolating and quantifying sources of heterogeneity.

Nano-engineered particle motion is inherently stochastic due to the fundamental length scales involved in the transport process [3,12]. As such, the measured particle dose per cell will be distributed according to the transport properties, as well as any potential heterogeneity in cell characteristics. Without careful consideration of the contribution of the stochastic nature of transport to the dosage distribution, heterogeneity in cell characteristics can be misidentified or incorrectly estimated. Mathematical models of particle motion are effective at isolating the contribution of particle transport to dosage from biological interactions [3,5,7–9]. However, such models describe the average particle behaviour and dose, and are not suitable for predicting dosage distributions or cell heterogeneity. Statistical approaches allow for the quantification of heterogeneity from experimental data [10,11,14], but do not provide mechanistic understanding about how heterogeneity in experimental data arises from heterogeneity in multiple cell characteristics. Furthermore, as we will demonstrate, conclusions obtained from previous statistical approaches are incapable of explaining heterogeneity observed in our time course experiments.

2. Results

Here, we develop and introduce a model of individual nano-engineered particle behaviour that is capable of describing and predicting cell heterogeneity. This modelling framework mimics experimental conditions while providing detail at both an individual particle and individual cell level. The standard experimental approach for analysing particle–cell interactions is an adherent cell culture association assay [7]. In an association assay, a cell population seeded on a culture dish is incubated in media containing a particle suspension (figure 1) [7]. The particles undergo transport through the fluid via a combination of sedimentation and diffusion, and ultimately arrive at the cell–media interface (figure 2*c*,*e*–*g*) [3,7–9]. Particles bind to receptors on the cell surface and are internalized via various endocytic processes [4]. The evolution of the number of particles associated with each cell is measured to provide time course information on the dose (figure 2*d*). It is difficult to distinguish between particles that are internalized by a cell or are merely bound to the cell surface, and hence we take the standard approach of using the number of associated particles as a proxy for dose [8,21]. Owing to the ubiquitous use of association experiments to investigate particle efficacy, we calibrate the geometry and conditions in our modelling framework to an association assay.

We implement a voxel-based framework, where the experimental domain is discretized into cube-shaped subdomains known as voxels (figure 2*a*,*b*). We model the number of particles within each voxel, which evolves with time due to stochastic transitions of particles between voxels. The transition rates correspond to the combined rates of sedimentation and diffusion [22]. Transition events are sampled via a spatial stochastic simulation algorithm, a modified form of the well-established Gillespie's algorithm [23]. To replicate experimental conditions, there is no transition of particles through the top of the domain, corresponding to the air-media interface. At the cell–media interface, the transition rate of particles from the media into the cell monolayer corresponds to the cell carrying capacity kinetics derived by Faria *et al.* [8]. These kinetics have been demonstrated to be the most suitable kinetics for describing association assays for a wide range of particle–cell combinations [8]. The kinetics rely on two parameters: a *particle–cell affinity* parameter, which represents the rate of interaction between a particle and a cell, and a *cell carrying capacity* parameter, which is the maximum number of particles that can associate with a cell [8]. Note that the affinity parameter does not imply a specific type of particle–cell association, such as clathrin-mediated endocytosis or macropinocytosis. Instead, the affinity parameter is an abstraction of the combined effect of all binding and internalization processes. As such, the

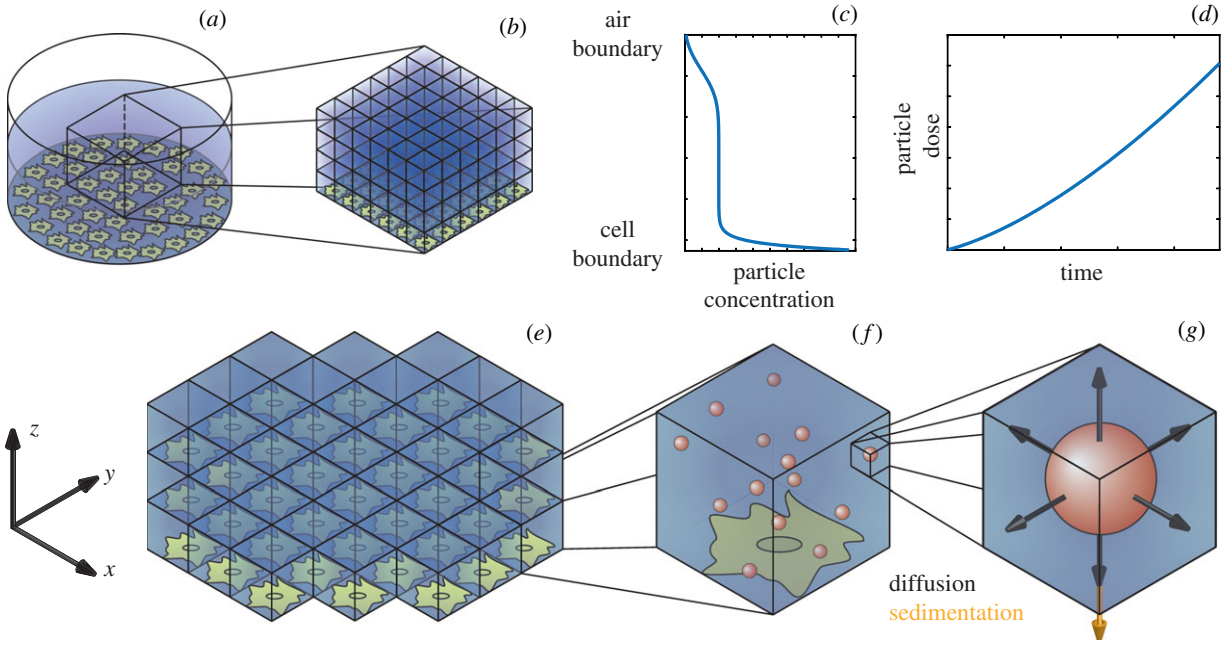

Figure 2. Experimental and model geometry. (*a*) Standard experimental geometry for an *in vitro* adherent cell culture association assay. (*b*) Representative geometry for the voxel-based modelling framework. (*c*) Typical particle concentration as a function of depth due to sedimentation and diffusion of particles. (*d*) Typical particle association curve. (*e*) Media–cell boundary in the modelling framework highlighting (*f*) particle locations within a voxel and (*g*) the contributions of random motion (diffusion) and directed motion (sedimentation) to particle transport.

modelling framework is applicable across a range of particle sizes, even though the dominant biological process governing particle–cell association changes with particle size [1,8]. Full details of the voxel-based model, the equivalence of the transition rate used here to the cell carrying capacity kinetics of Faria *et al.* [8], and an efficient method to calculate the average behaviour in the voxel-based model are derived in the electronic supplementary material [22,24].

2.1. Stochastic motion does not account for all observed variation

Our modelling framework describes both individual particles and individual cells and, therefore, we are able to explicitly measure the number of particles associated with each cell. As particle motion is stochastic, the model output will be a distribution of particles per cell. This distribution can be readily compared with experimental data, as flow cytometry techniques can be used to measure the number of particles associated with each cell for an entire cell population [25–27].

Experimentally, even when all cells have identical characteristics, the number of particles per cell will be heterogeneous due to the inherent stochasticity of particle motion. This dosage distribution is dependent on the association regime of the cells. For example, if the cells are in the linear association regime, where the number of particles per cell is significantly lower than the carrying capacity, then the dosage distribution will be Poisson distributed with an arrival rate equivalent to the average association rate of particles with the cell layer. However, this may not be the case when the particle dose is close to the maximum number of particles per cell.

To determine the influence of stochastic transport on the particle dosage distribution, we perform simulations using our modelling framework and calculate the number of particles associated with each cell. Here, we first consider idealized conditions where all cells in an experiment have identical characteristics. These simulations are calibrated to match three different experiments: the first is performed with 1032 nm PMA_{SH} capsule particles and RAW264.7 cells, the second is performed with 282 nm PMA_{SH} coreshell particles and HeLa cells, and the third is performed with 150 nm PMA_{SH} coreshell particles and RAW264.7 cells [8,28]. Full experimental details can be found in the electronic supplementary material.

As noted previously, the dose obtained from the model is only Poisson distributed in the linear association regime (electronic supplementary material, figure S1). If the number of particles per cell approaches the carrying capacity, the predicted dosage distribution is not well described by the Poisson distribution. Comparing the dosage distribution obtained from the model with the experimental data, we observe that the experimental data is overdisperse compared to the model predictions (electronic supplementary material, figure S1). This indicates that the cell populations exhibit heterogeneity, and is consistent with previous observations [10–14].

2.2. Heterogeneity is time-dependent

Having established that the experimental data are not consistent with a homogeneous cell population, we next consider implementing heterogeneity in our modelling framework. A natural choice is to allow each cell in the model to have a particle–cell affinity parameter that is sampled from a probability distribution. This represents variation in the biological processes that dictate particle association, such as the number of receptors or vesicle formation rates [11]. Lognormal distributions are prevalent throughout biology, and arise from multiplicative sources of variability [3,13,29]. As such, here we make the assumption that affinity is lognormally distributed. Note that other distributions could be considered, and while this would affect the final dosage distribution, the analysis techniques remain the same.

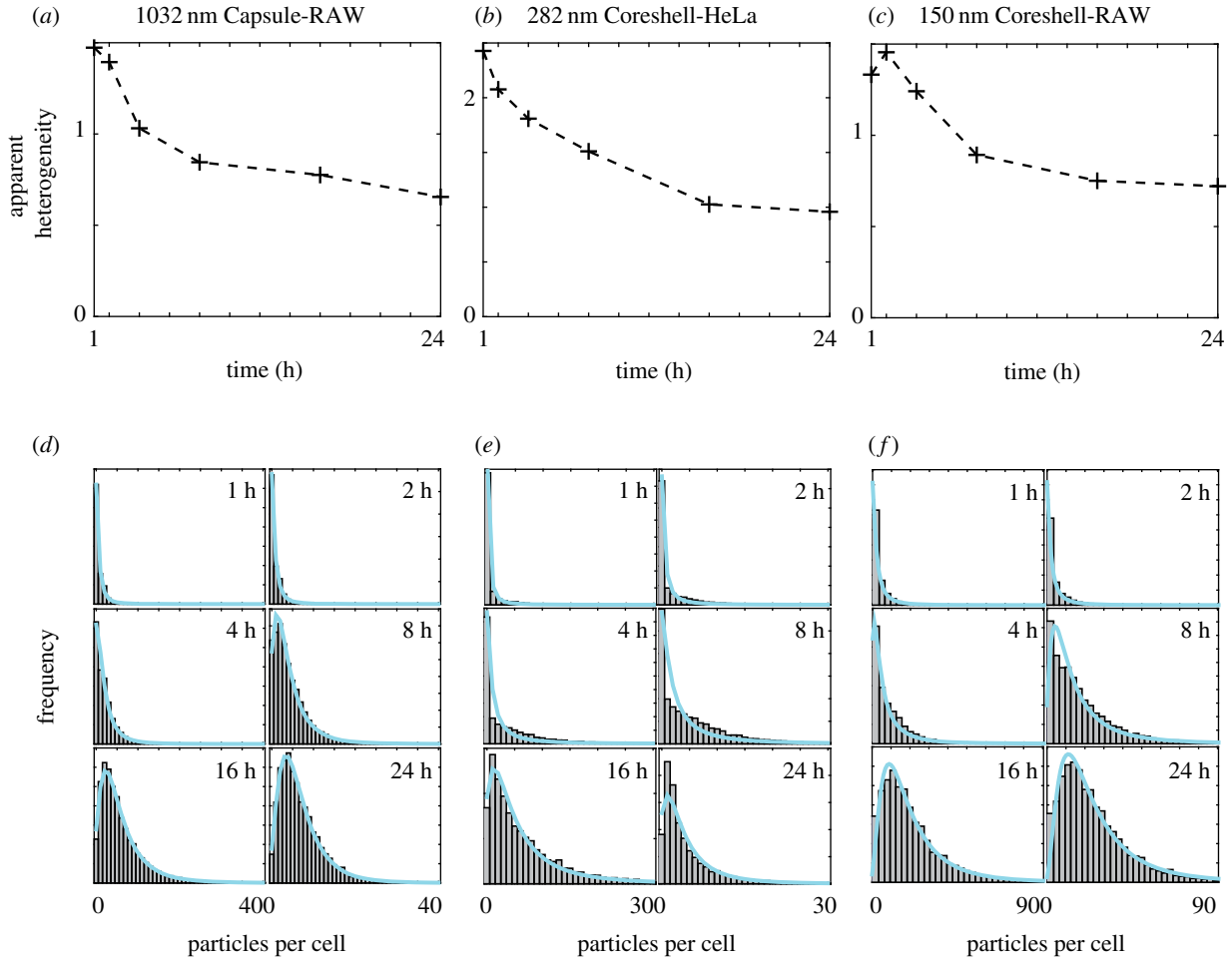

Figure 3. Heterogeneity appears to change with time. (*a–c*) Evolution of apparent heterogeneity obtained from experimental data for three particle–cell pairs. (*d–f*) Dosage distributions for the three particle–cell pairs after 1, 2, 4, 8, 16 and 24 h. The cyan line corresponds to the Poisson-lognormal distribution that best fits the dosage distribution.

As each cell now has an individual affinity parameter, and the association rate for each cell is proportional to the affinity, the number of particles per cell will follow a Poisson-lognormal distribution [30] (electronic supplementary material). Critically, this allows us to determine the relative contributions of stochastic particle motion and cell heterogeneity to the variation in the dosage distribution. The applicability of the Poisson-lognormal distribution relies on the assumption that the number of particles associated with a cell is independent of other cells; that is, competition between cells for particles is minimal. This is appropriate provided that association occurs sufficiently slowly compared to particle transport, as is the case for the particle–cell combinations considered here. There is only a single free parameter in the distribution, the standard deviation, as the mean of the Poisson-lognormal distribution must correspond to the mean number of associated particles. We refer to this standard deviation as the 'apparent heterogeneity.'

The apparent heterogeneity is a key concept for the work presented here. As the dosage distribution is described by the Poisson-lognormal distribution, the heterogeneity present in the data is captured via the measure of spread in the Poisson-lognormal distribution: the standard deviation (apparent heterogeneity). It is important to note that this is not the 'true' heterogeneity in one (or more) of the cell characteristics. Rather, the apparent heterogeneity represents how the 'true' heterogeneity manifests itself in the experimental dosage distribution. As the particle dose can be indicative of therapeutic success, it is therefore necessary to understand how the apparent heterogeneity arises from the 'true' heterogeneity in the cell characteristics.

To examine the apparent heterogeneity present in the experimental data, we fit the Poisson-lognormal distribution to the experimental data at each measured time point. In figure 3, we present both the distribution fit and the evolution of the apparent heterogeneity. Figure 3*d–f* shows that the Poisson-lognormal describes the data well for all three experiments, indicating that the assumption of lognormally distributed cell characteristics is appropriate. Notably, the apparent heterogeneity changes with time (figure 3*a–c*). For each particle–cell pair, the apparent heterogeneity decreases rapidly at early time before beginning to plateau towards the final experimental observation. This observation suggests that previous investigations into heterogeneity in particle–cell interactions, where the heterogeneity is assumed to be constant [11], do not represent a complete picture due to the time-dependent nature of particle–cell interactions. Therefore, we next seek to determine how the time dependence of apparent heterogeneity arises as a consequence of interactions between particles and various cell characteristics.

2.3. Cell size distribution does not account for time-dependent heterogeneity

To determine whether the experimental apparent heterogeneity arises solely from heterogeneous particle–cell association,

as suggested previously [11], we introduce cell heterogeneity into our modelling framework via the affinity parameter. A potential explanation for heterogeneous affinity is the heterogeneity in cell surface area due to the cell cycle [11,31,32]. Specifically, we assume that a cell with higher surface area is more likely to interact and associate with particles [11]. We calibrate a lognormal distribution to the square of small-angle light scattering intensity obtained via flow cytometry for both HeLA and RAW264.7 cells to estimate the cell surface area heterogeneity [33]. This heterogeneity is used to create the lognormal distribution for the affinity parameter. We note that the cell morphology may be different for cells in suspension in the flow cytometer, compared to cells adhering to the culture dish. As such, obtaining estimates of cell surface area distributions via *in situ* microscopy images of the adherent cell culture, as in [11], may represent an area of potential improvement for the experimental protocol. However, such an improvement would only impact the accuracy of the affinity parameter, which is not the main focus of this work.

We perform simulations representing the three previously described experiments, now incorporating heterogeneous particle–cell affinity, and present the results in figure 4*a–f*. To obtain robust estimates of the apparent heterogeneity, we use an efficient approach that provides the average particle dose for each cell, and fit the Poisson-lognormal distribution to this dosage data. This approach provides results that are consistent with the average output of the voxel-based model (electronic supplementary material, figure S3), and avoids fluctuations in the apparent heterogeneity due to the stochastic nature of the voxel-based model.

As predicted, the dosage distribution obtained from the model is Poisson-lognormal distributed in the linear association regime, but does not follow the Poisson-lognormal distribution near the carrying capacity. For the simulation of the experiment that remains in the linear association regime (figure 4*d*) the apparent heterogeneity stays close to the 'true' heterogeneity in the cell characteristics, that is the standard deviation of the particle–cell affinity distribution (figure 4*a*). For the simulation of the two experiments where the number of particles per cell approaches the carrying capacity (figure 4*e,f*), the apparent heterogeneity decreases as time increases, even though the 'true' heterogeneity is constant (figure 4*b,c*).

While this is a potential explanation for the decrease in apparent heterogeneity observed experimentally, the model predicts that the apparent heterogeneity approaches zero as time increases, whereas the apparent heterogeneity in the experimental data appears to approach a finite positive value (figure 3). Further, the time dependence in the apparent heterogeneity obtained from the model results from a breakdown in the match between the dosage distribution and the Poisson-lognormal distribution as the number of particles per cell approaches the carrying capacity (figure 4*d–f*). By contrast, the experimental dosage distribution is well described by the Poisson-lognormal distribution in all cases, even though the number of particles per cell approaches the carrying capacity in the 282 nm coreshell-HeLa and 150 nm coreshell-RAW264.7 experiments (figure 3). This suggests that the model assumption of a homogeneous carrying capacity is incompatible with the experimental data.

An increase in cell surface area may increase the maximum number of particles that can associate with a cell. As such, we now impose a lognormal distribution on the cell carrying capacity parameter, where this lognormal distribution has the same standard deviation as the cell surface area distribution. We make the assumption that the particle–cell affinity and cell carrying capacity parameters are correlated, that is a cell with higher affinity due to a higher surface area will also have a higher carrying capacity. We perform simulations, again representing the three previously described experiments, with heterogeneous particle–cell affinity and heterogeneous cell carrying capacity, and present the results in figure 4*g–l*. The apparent heterogeneity is consistent with the cell surface area heterogeneity in each case (figure 4*g–i*), and the model dosage distributions are all described well by the Poisson-lognormal distribution (figure 4*j–l*). However, the model-predicted apparent heterogeneity due to the variation in cell surface area is constant with respect to time, and therefore insufficient to explain the evolution in the apparent heterogeneity obtained from the experimental data.

2.4. Cell cycle does not introduce time-dependent heterogeneity

The previous results assumed that the cells present in the population are representative of all phases within the cell cycle. To investigate whether the progression through the cell cycle during the experiment affects the apparent heterogeneity, we now incorporate the cell cycle explicitly in our modelling framework. We implement a multistage model of cell cycle progression, where cells exist in one of m states, representing different phases of the cell cycle [34]. Cells transition between states at rates corresponding to the average time spent in a particular phase. Here, we choose $m = 4$, corresponding to the G1, S, G2 and M phases. We consider two approaches for introducing heterogeneity. First, we impose cell heterogeneity via a lognormal distribution as previously. Second, we introduce a phase-specific mean affinity parameter, representing the change in cell size between phases. The standard deviation is independent of phase. When a cell transitions from M phase to G1 phase, and undergoes mitosis, an additional cell is introduced. The daughter cell either inherits the original cell's affinity parameter, or has the G1 phase affinity parameter, depending on the cell cycle approach considered. The particle load of the original cell is split evenly between the original cell and the daughter cell. Full details of the cell cycle model can be found in the electronic supplementary material.

We perform simulations representing the three experiments described previously, with the addition of the two approaches for modelling heterogeneity via cell cycle progression, ensuring that the mean affinity is consistent with the previous model simulations. The efficient approach used above to obtain the average particle dose per cell cannot be used here to obtain the apparent heterogeneity as cell behaviour must be explicitly described, and as such we revert to the full voxel-based model. For both approaches, we observe that the apparent heterogeneity is relatively consistent, though slightly reduced, compared to the true heterogeneity in the cell characteristics (figure 5*a–c*). This slight reduction is associated with mitosis; splitting the particle load into two cells reduces the number of cells carrying high numbers of particles. In both cases, the apparent heterogeneity is approximately constant over time, unlike the experimental data, which indicates that the cell cycle cannot explain the apparent evolution of heterogeneity in particle dosage distributions. The choice of modelling approach does not significantly influence either the apparent

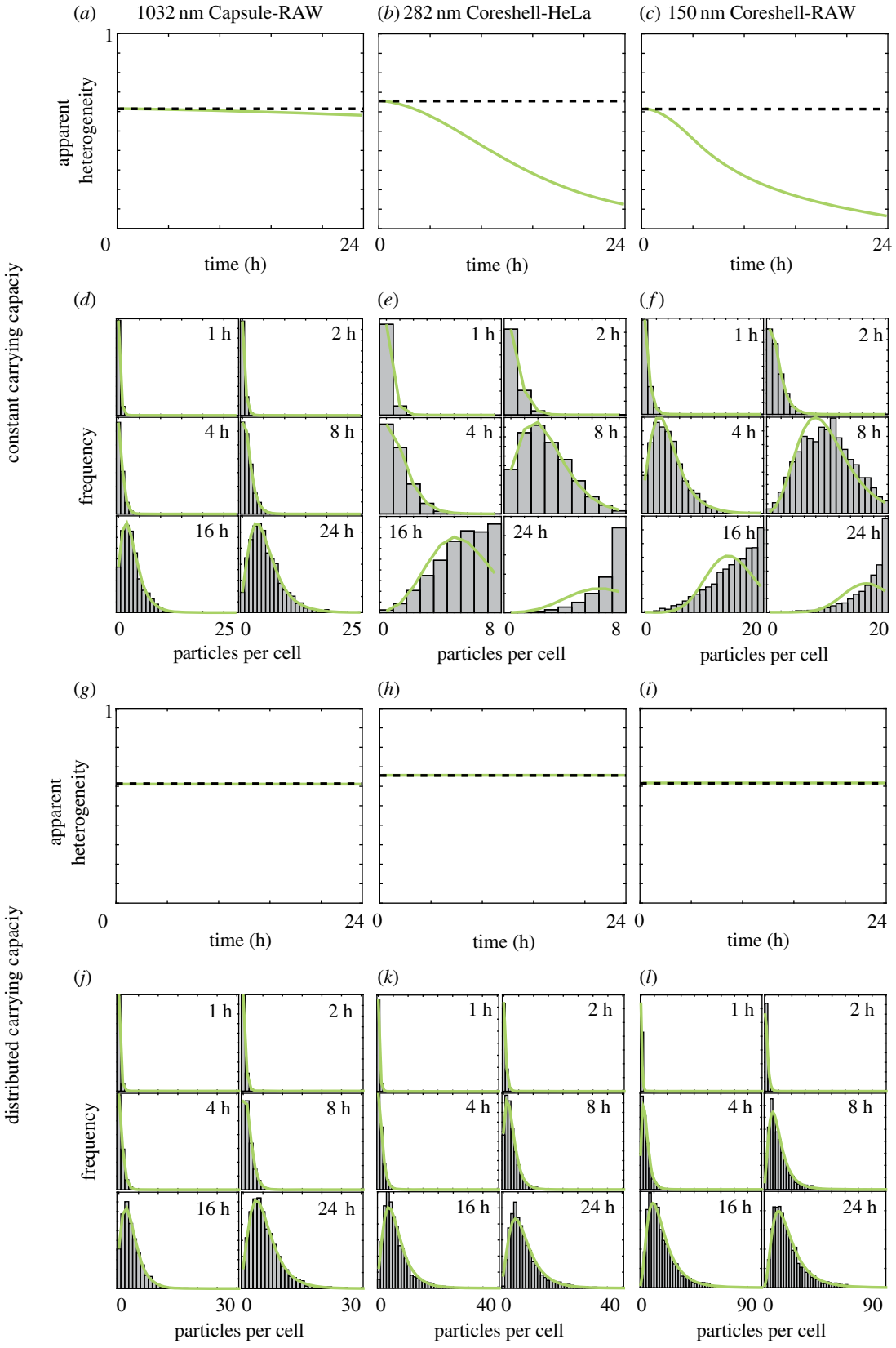

Figure 4. Cell size distribution does not explain changes in heterogeneity. (*a–c*), (*g–i*) Evolution of apparent heterogeneity obtained from the modelling framework for three particle–cell pairs. The affinity parameter for each cell is sampled from a lognormal distribution with a standard deviation corresponding to the dashed black line. The cell carrying capacity parameter is either (*a–c*) constant or (*g–i*) lognormally distributed with a standard deviation corresponding to the dashed black line. (*d–f*), (*j–l*) Dosage distributions for the three particle–cell pairs after 1, 2, 4, 8, 16 and 24 h obtained from the voxel-based model. The green line corresponds to the Poisson-lognormal distribution that best fits the dosage distribution.

heterogeneity or the dosage distribution, as highlighted in figure 5*a–c* and *d–i*, respectively. Therefore, we do not consider the cell cycle in the remainder of this work. The results presented in figures 4 and 5 clearly demonstrate that conclusions drawn from previous investigations [10,11,14] into the sources of particle–cell heterogeneity are incomplete, and are incapable of explaining the observed time-dependence of heterogeneity in particle dosage.

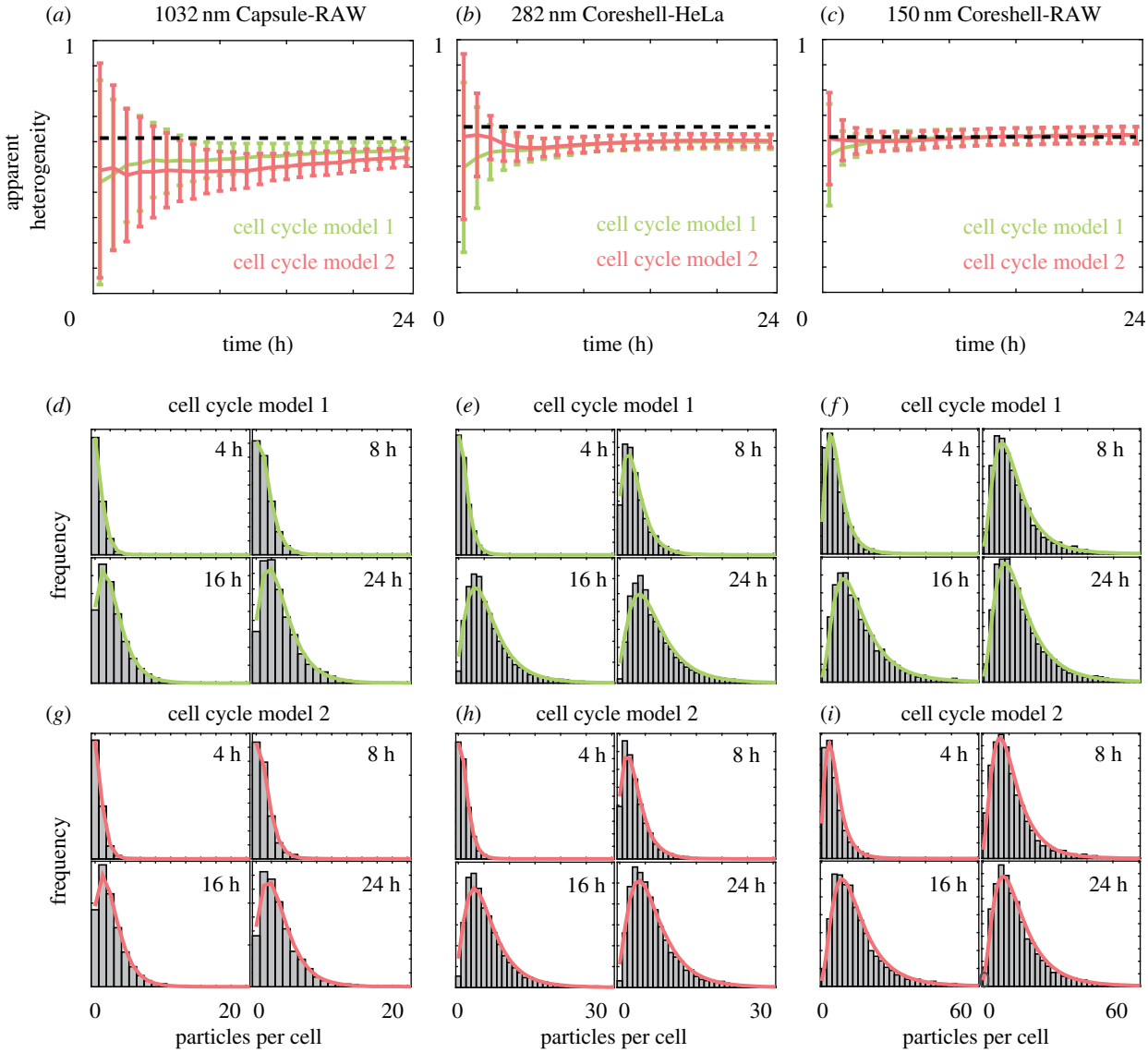

Figure 5. Cell cycle progression does not explain changes in heterogeneity. (*a–c*) Evolution of the average apparent heterogeneity obtained from 200 realizations of the voxel-based framework for the three particle–cell pairs if the cell cycle is included in the framework via Model 1 (green) and Model 2 (pink). Error bars correspond to one standard deviation. The dashed black line corresponds to the affinity and capacity heterogeneity. (*d–i*) Dosage distributions for the three particle–cell pairs after 4, 8, 16 and 24 h obtained from the voxel-based model for (*d–f*) Model 1 and (*g–i*) Model 2. The (*d–f*) green and (*g–i*) pink lines correspond to the Poisson-lognormal distribution that best fit the dosage distribution.

2.5. Interplay between nano-engineered particle motion, affinity heterogeneity and capacity heterogeneity determines apparent heterogeneity

The association of particles with cells is eventually restricted by the cell carrying capacity [8]. As highlighted by the results in figure 4, the heterogeneity in the carrying capacity cannot be neglected. As multiple biological factors may induce heterogeneity in particle–cell affinity or cell carrying capacity, the amount of heterogeneity may differ between different cell characteristics. Therefore, we now relax the assumption that both the cell carrying capacity and the particle–cell affinity are distributed with the same degree of heterogeneity. To determine the heterogeneity for both cell carrying capacity and particle–cell affinity we iteratively calibrate the modelling framework to both the mean particle dose and the apparent heterogeneity obtained from the experimental data. This allows us to extract estimates of the heterogeneity in the cell carrying capacity and the particle–cell affinity, while ensuring that the mean dosage is consistent with the experimental data, as shown in figure 6. For each experimental dosage curve, we observe that the model accurately describes the mean experimental dose. By varying the particle–cell affinity heterogeneity and cell carrying capacity heterogeneity independently we are able to match the evolution of the apparent heterogeneity obtained from the experimental data.

At early time, where the rate of particle association predominantly depends on the particle–cell affinity, the apparent heterogeneity is close to the 'true' heterogeneity in the affinity parameter (1.42, 3.05 and 1.71 in figure 6*a–c*, respectively). As time progresses, the number of associated particles per cell becomes more dependent on cell carrying capacity. Therefore, we observe that the apparent heterogeneity decreases and approaches the 'true' heterogeneity in the cell carrying capacity parameter (0.61, 0.62 and 0.75 in figure 6*a–c*, respectively). This transition demonstrates how these two sources of heterogeneity interact and, consequently, how the 'true' heterogeneity manifests itself in the experimental dosage data. All three sources of heterogeneity, namely the stochastic particle motion, variation in particle–cell affinity and variation in cell

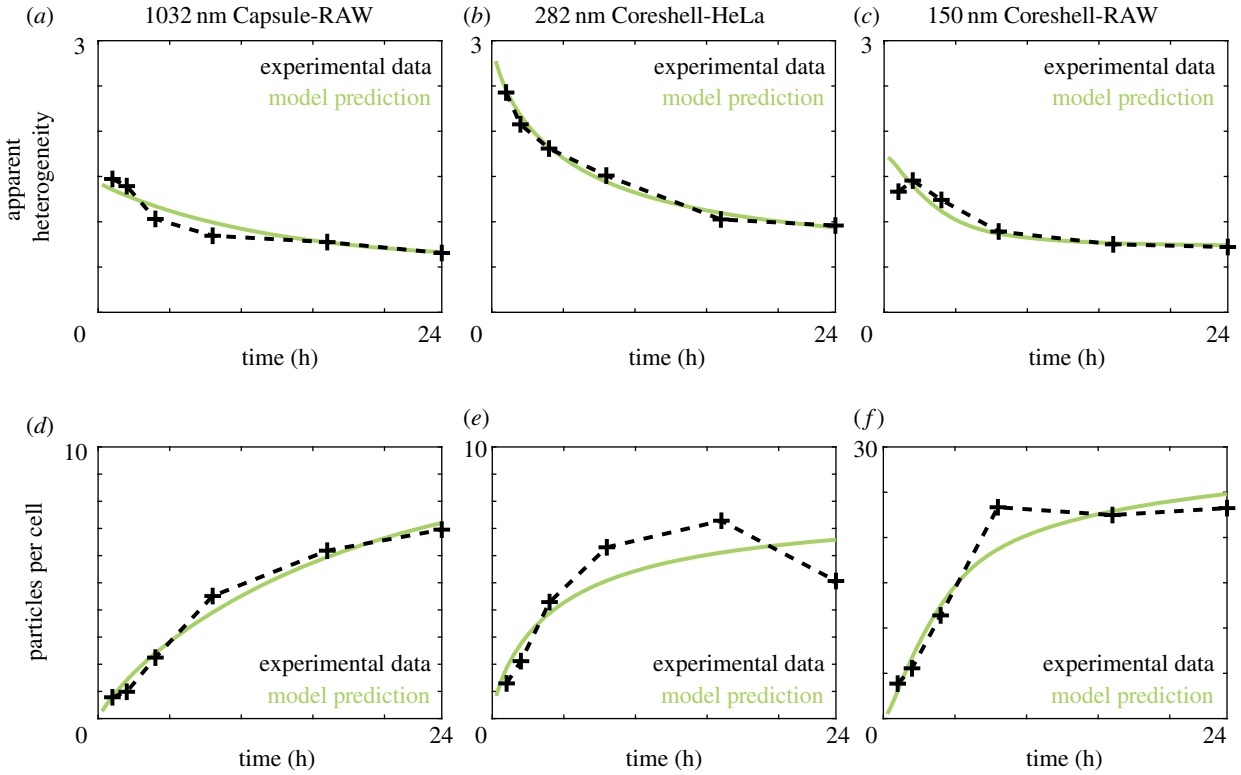

Figure 6. Combining stochastic transport, particle–cell affinity heterogeneity and cell carrying capacity heterogeneity explains experimentally observed heterogeneity. Comparison between the model predictions (green) and experimental data (black) for (*a–c*) apparent heterogeneity and (*d–f*) number of particles per cell for the three particle–cell combinations. Here, the heterogeneity in particle–cell affinity is different to the heterogeneity in cell carrying capacity.

carrying capacity, are thus required to explain the heterogeneity in the experimental dosage distributions. Critically, the heterogeneity in the particle–cell affinity is different to the heterogeneity in the cell carrying capacity. Without this difference in heterogeneity between the two cell parameters, we do not observe the change in the apparent heterogeneity over time.

3. Discussion and conclusion

Experimental data obtained from nano-engineered particle–cell association assays exhibit variation in the number of particles associated per cell. We demonstrate that this variation arises from a combination of stochastic particle transport and heterogeneity in cell characteristics. In particular, heterogeneity in the affinity between particles and cells, and heterogeneity in the maximum number of associated particles per cell are shown to be the key biological processes driving variation in experimental data. The amount of variation in the experimental data appears to change with time, but we demonstrate that this is a consequence of different amounts of heterogeneity in these two biological processes.

Uncovering the biological and physical mechanisms that impact the ability of specific cells to associate with, and subsequently internalize, nano-engineered particles is necessary for informed particle design [1,2,8]. The ability to reliably deliver particles to a target cell population such that the particles are rapidly internalized has the potential to transform disease treatment and diagnosis [35–37]. However, the journey between particle creation and cellular internalization is convoluted, and involves a multitude of intertwined biological, physical and chemical processes [1–4,8]. The combination of this complex tapestry with heterogeneous experimental data has thus far inhibited understanding of the key mechanisms governing particle–cell interactions.

Here we develop a mathematical framework of individual-level particle–cell interactions that can be used to separate the physical processes governing particle transport from the biological processes dictating the cellular uptake of nano-engineered particles. We employ this framework to explain the apparent temporal evolution of heterogeneity within a cell population. This apparent evolution is driven by the interplay between the inherent stochastic motion of the particles, the heterogeneity in the maximum number of particles internalized by a particular cell, and the heterogeneity in the affinity between the particles and the cells. When considered in isolation, these three processes are unable to describe the apparent evolution in heterogeneity present in the experimental data. All three sources of heterogeneity in concert are necessary to explain the experimental data. Further, we demonstrate the impact of the cell cycle is insufficient to explain the heterogeneity in particle dose. This is in contrast to results obtained from a recent investigation [11], where it was claimed that the combination of stochastic particle motion and the distribution of cell surface area is sufficient to explain the heterogeneity in particle dosage. While this explanation is valid for the short-time experiments performed in [11], we conclusively demonstrate, using our modelling framework and performing experiments over a longer time period, that this combination does not give rise to the experimental observation that heterogeneity that changes over time. This has important implications for understanding the impact of heterogeneity, as our modelling approach reveals that the critical biological mechanism inducing heterogeneity in particle dosage changes over time.

By recognizing that early-time particle–cell association is driven by particle–cell affinity and that late-time particle–cell association is governed by the cell carrying capacity, we provide an intuitive explanation for the apparent evolution of heterogeneity in the experimental data. That is, the apparent heterogeneity is equal to the particle–cell affinity heterogeneity at early time, and will transition to the cell carrying capacity heterogeneity over time, at a rate corresponding to the particle transport and association rate.

Extracting reliable estimates of the true heterogeneity in cell characteristics is critical for therapeutic purposes [13,19,20]. If only a fraction of a cell population appears to internalize a therapeutic dose of particles, it is crucial to determine whether this is due to stochastic interactions or an underlying biological process. The former implies that increasing the dosage or exposure time will increase the fraction of the population that are effectively treated, whereas the latter suggests that an alternative treatment protocol may be required. Furthermore, the cells that do have lower particle affinity, and a lower carrying capacity, are more likely to not internalize particles (electronic supplementary material, figure S9). This imposes a selective pressure on the cell population toward lower particle–cell affinity and cell carrying capacity values, as such cells do not respond to the particle treatment.

The framework presented here demonstrates that mechanistic modelling approaches can be employed to isolate the sources of heterogeneity present in a cell population from particle–cell association data. Subsequently, this provides insight into whether cell subpopulations exist, and the degree to which such subpopulations are resistant to treatment. More generally, this work highlights how mechanistic insight can be used to explain the presence and origin of heterogeneity in experimental data. The influence of cell heterogeneity is a current question of interest across a diverse range of fields, including cancer biology [19,20], molecular biology [38], nanomedicine [11,14] and microbiology [39]. Mechanistic models that incorporate heterogeneity and examine its associated impact, such as the one presented here, may provide the key required to understand the influence of cell heterogeneity.

4. Material and methods

Detailed information regarding the mathematical framework and experimental protocol can be found in the electronic supplementary material.

Data accessibility. Certain experimental data used in this analysis have been previously published [8] and raw data are available at https://figshare.com/projects/In_vitro_cell-particle_association/59162. The code used to implement the mathematical framework is available at https://github.com/DrStuartJohnston/nanoparticle-cell-interactions.

Authors' contributions. S.T.J. conceived the study. S.T.J., M.F. and E.J.C. designed the numerical experiments. S.T.J. designed and performed the analysis. S.T.J. wrote the manuscript. S.T.J., M.F. and E.J.C. edited the manuscript. All authors gave final approval for publication.

Competing interests. The authors declare that there are no conflicts of interest.

Funding. This research was in part conducted and funded by the Australian Research Council Centre of Excellence in Convergent Bio-Nano Science and Technology (project no. CE140100036). S.T.J. is supported by the Australian Research Council (project no. DE200100988).

Acknowledgements. The authors thank the anonymous referees for their helpful feedback.

References

1. Albanese A, Tang PS, Chan WC. 2012 The effect of nanoparticle size, shape, and surface chemistry on biological systems. *Annu. Rev. Biomed. Eng* **14**, 1–16. (doi:10.1146/annurev-bioeng-071811-150124)
2. Li Y, Lian Y, Zhang LT, Aldousari SM, Hedia HS, Asiri SA, Liu WK. 2016 Cell and nanoparticle transport in tumour microvasculature: the role of size, shape and surface functionality of nanoparticles. *Interface Focus* **6**, 20150086. (doi:10.1098/rsfs.2015.0086)
3. Johnston ST, Faria M, Crampin EJ. 2018 An analytical approach for quantifying the influence of nanoparticle polydispersity on cellular delivered dose. *J. R. Soc. Interface* **15**, 20180364. (doi:10.1098/rsif.2018.0364)
4. Richards DM, Endres RG. 2016 Target shape dependence in a simple model of receptor-mediated endocytosis and phagocytosis. *Proc. Natl Acad. Sci. USA* **113**, 6113–6118. (doi:10.1073/pnas.1521974113)
5. Björnmalm M, Faria M, Chen X, Cui J, Caruso F. 2016 Dynamic flow impacts cell–particle interactions: sedimentation and particle shape effects. *Langmuir* **32**, 10 995–11 001. (doi:10.1021/acs.langmuir.6b03216)
6. Food and Drug Administration. 2014 Considering whether an FDA-regulated product involves the application of nanotechnology. FDA-2010-D-0530.
7. DeLoid GM, Cohen JM, Pyrgiotakis G, Demokritou P. 2017 Preparation, characterization, and *in vitro* dosimetry of dispersed, engineered nanomaterials. *Nat. Protoc.* **12**, 355–371. (doi:10.1038/nprot.2016.172)
8. Faria M, Noi KF, Dai Q, Björnmalm M, Johnston ST, Kempe K, Caruso F, Crampin EJ. 2019 Revisiting cell–particle association *in vitro*: a quantitative method to compare particle performance. *J. Control Release* **307**, 355–367. (doi:10.1016/j.jconrel.2019.06.027)
9. Hinderliter PM, Minard KR, Orr G, Chrisler WB, Thrall BD, Pounds JG, Teeguarden JG. 2010 ISDD: a computational model of particle sedimentation, diffusion and target cell dosimetry for *in vitro* toxicity studies. *Part Fibre Toxicol.* **7**, 36. (doi:10.1186/1743-8977-7-36)
10. Jeynes JCG, Jeynes C, Merchant MJ, Kirkby KJ. 2013 Measuring and modelling cell-to-cell variation in uptake of gold nanoparticles. *Analyst* **138**, 7070–7074. (doi:10.1039/c3an01406a)
11. Rees P, Wills JW, Brown MR, Barnes CM, Summers HD. 2019 The origin of heterogeneous nanoparticle uptake by cells. *Nat. Commun.* **10**, 2341. (doi:10.1038/s41467-019-10112-4)
12. Summers HD, Rees P, Holton MD, Brown MR, Chappell SC, Smith PJ, Errington RJ. 2011 Statistical analysis of nanoparticle dosing in a dynamic cellular system. *Nat. Nanotechnol.* **6**, 170. (doi:10.1038/nnano.2010.277)
13. Turnbull T *et al.* 2019 Cross-correlative single-cell analysis reveals biological mechanisms of nanoparticle radiosensitization. *ACS Nano* **13**, 5077–5090. (doi:10.1021/acsnano.8b07982)
14. Ware MJ, Godin B, Singh N, Majithia R, Shamsudeen S, Serda RE, Meissner KE, Rees P, Summers HD. 2014 Analysis of the influence of cell heterogeneity on nanoparticle dose response. *ACS Nano* **8**, 6693–6700. (doi:10.1021/nn502356f)
15. Altschuler SJ, Wu LF. 2010 Cellular heterogeneity: do differences make a difference? *Cell* **141**, 559–563. (doi:10.1016/j.cell.2010.04.033)
16. Lambert B, Gavaghan DJ, Tavener S. 2019 A Monte Carlo method to estimate cell population heterogeneity. *bioRxiv* 758284. (doi:10.1101/758284)
17. Waldherr S. 2018 Estimation methods for heterogeneous cell population models in systems biology. *J. R. Soc. Interface* **15**, 20180530. (doi:10.1098/rsif.2018.0530)
18. Teeguarden JG, Hinderliter PM, Orr G, Thrall BD, Pounds JG. 2006 Particokinetics *in vitro*: dosimetry considerations for *in vitro* nanoparticle toxicity assessments. *Toxicol. Sci.* **95**, 300–312. (doi:10.1093/toxsci/kfl165)

19. Greaves M, Maley CC. 2012 Clonal evolution in cancer. *Nature* **481**, 306. (doi:10.1038/nature10762)
20. Sottoriva A, Spiteri I, Piccirillo SG, Touloumis A, Collins VP, Marioni JC, Curtis C, Watts C, Tavaré S. 2013 Intratumor heterogeneity in human glioblastoma reflects cancer evolutionary dynamics. *Proc. Natl Acad. Sci. USA* **110**, 4009–4014. (doi:10.1073/pnas.1219747110)
21. Johnston AP. 2017 Life under the microscope: quantifying live cell interactions to improve nanoscale drug delivery. *ACS Sensors* **2**, 4–9. (doi:10.1021/acssensors.6b00725)
22. Noel A, Makrakis D. 2018 Algorithm for mesoscopic advection–diffusion. *IEEE Trans. Nanobiosci.* **17**, 543–554. (doi:10.1109/TNB.2018.2878065)
23. Gillespie DT. 1977 Exact stochastic simulation of coupled chemical reactions. *J. Phys. Chem.* **81**, 2340–2361. (doi:10.1021/j100540a008)
24. Erban R, Chapman SJ. 2007 Reactive boundary conditions for stochastic simulations of reaction–diffusion processes. *Phys. Biol.* **4**, 16. (doi:10.1088/1478-3975/4/1/003)
25. Gottstein C, Wu G, Wong BJ, Zasadzinski JA. 2013 Precise quantification of nanoparticle internalization. *ACS Nano* **7**, 4933–4945. (doi:10.1021/nn400243d)
26. Steinkamp JA, Wilson JS, Saunders GC, Stewart CC. 1982 Phagocytosis: flow cytometric quantitation with fluorescent microspheres. *Science* **215**, 64–66. (doi:10.1126/science.7053559)
27. Varela JA, Bexiga MG, Åberg C, Simpson JC, Dawson KA. 2012 Quantifying size-dependent interactions between fluorescently labeled polystyrene nanoparticles and mammalian cells. *J. Nanobiotechnol.* **10**, 39. (doi:10.1186/1477-3155-10-39)
28. Kempe K, Noi KF, Ng SL, Müllner M, Caruso F. 2014 Multilayered polymer capsules with switchable permeability. *Polymer* **55**, 6451–6459. (doi:10.1016/j.polymer.2014.09.074)
29. Limpert E, Stahel WA, Abbt M. 2001 Log-normal distributions across the sciences: keys and clues: on the charms of statistics, and how mechanical models resembling gambling machines offer a link to a handy way to characterize log-normal distributions, which can provide deeper insight into variability and probability–normal or log-normal: that is the question. *Bioscience* **51**, 341–352. (doi:10.1641/0006-3568(2001)051[0341:LNDATS]2.0.CO;2)
30. Bulmer M. 1974 On fitting the Poisson lognormal distribution to species-abundance data. *Biometrics* **30**, 101–110. (doi:10.2307/2529621)
31. Kim JA, Åberg C, Salvati A, Dawson KA. 2012 Role of cell cycle on the cellular uptake and dilution of nanoparticles in a cell population. *Nat. Nanotechnol.* **7**, 62. (doi:10.1038/nnano.2011.191)
32. Panet E, Mashriki T, Lahmi R, Jacob A, Ozer E, Vecsler M, Lazar I, Tzur A. 2017 The interface of nanoparticles with proliferating mammalian cells. *Nat. Nanotechnol.* **12**, 598. (doi:10.1038/nnano.2017.140)
33. Shapiro HM. 2005 *Practical Flow Cytometry*. New Jersey: John Wiley & Sons.
34. Yates CA, Ford MJ, Mort RL. 2017 A multi-stage representation of cell proliferation as a Markov process. *Bull. Math. Biol.* **79**, 2905–2928. (doi:10.1007/s11538-017-0356-4)
35. Azzazy HM, Mansour MM. 2009 *In vitro* diagnostic prospects of nanoparticles. *Clin. Chim. Acta* **403**, 1–8. (doi:10.1016/j.cca.2009.01.016)
36. Kulkarni A *et al.* 2016 Reporter nanoparticle that monitors its anticancer efficacy in real time. *Proc. Natl Acad. Sci. USA* **113**, E2 104–E2 113. (doi:10.1073/pnas.1603455113)
37. Tavares AJ *et al.* 2017 Effect of removing Kupffer cells on nanoparticle tumor delivery. *Proc. Natl Acad. Sci. USA* **114**, E10 871–E10 880. (doi:10.1073/pnas.1713390114)
38. Snijder B, Pelkmans L. 2011 Origins of regulated cell-to-cell variability. *Nat. Rev. Mol. Cell Biol.* **12**, 119. (doi:10.1038/nrm3044)
39. Ackermann M. 2015 A functional perspective on phenotypic heterogeneity in microorganisms. *Nat. Rev. Microbiol.* **13**, 497. (doi:10.1038/nrmicro3491)